Chapter 5
Imaging for Detection of CSF Leaks

Marin Alisa McDonald

Introduction

A skull base cerebrospinal fluid (CSF) leak describes the egress of CSF from the intracranial subarachnoid space into the extracranial space via an osteodural defect, most commonly at the sinonasal or tympanomastoid cavities [1]. Leakage of CSF into either the nose or the ear, coined CSF rhinorrhea or otorrhea, was identified as pathologic entities over a century ago with a wide range of potential etiologies, including post-traumatic, surgical, neoplastic, and spontaneous causes. Subsequent decades have shown increasing recognition for the clinical importance of CSF leaks as sources of significant potential morbidity and mortality, with persistent CSF rhinorrhea carrying a 10 to 37% lifetime risk for meningitis [2–6], as well as increasing risk for seizures, cranial neuropathies, and headache [7].

Given the potential long-term consequences of missed diagnosis, the timely and accurate identification of a suspected CSF leak is of tremendous clinical import. β2-Transferrin protein testing remains the mainstay for confirmation of any suspected case of CSF rhinorrhea or otorrhea with reported sensitivity ranging from 87 to 100% and specificity of 71 to 94% [7–10]. Once confirmed, imaging plays a critical role in determining the site of a suspected or confirmed CSF leak, often using a combination of high-resolution computed tomography (HRCT) and magnetic resonance (MR) imaging, with or without the use of intrathecal contrast agents. Beyond the identification potential routes of CSF leak, radiological evaluation can also aid

M. A. McDonald (✉)
Division of Neuroradiology, Department of Radiology, University of California at San Diego, San Diego, CA, USA
e-mail: mamcdonald@health.ucsd.edu

E. C. Kuan et al. (eds.), *Skull Base Reconstruction*,
https://doi.org/10.1007/978-3-031-27937-9_5

in the diagnosis of any underlying causative etiology, such as spontaneous CSF leaks referable to idiopathic intracranial hypertension (IIH) or in the setting of skull base invasion from neoplastic or infectious etiologies [1, 7, 8, 11].

In the course of this chapter, we will review the imaging techniques used to diagnose and characterize the sites of CSF leak with an emphasis on noninvasive CT and MR imaging. We will highlight common imaging findings of confirmed CSF leaks and their causative factors, including traumatic, iatrogenic, and spontaneous leaks. We will then discuss potential mimics of CSF leak and common imaging pitfalls in this essential diagnosis.

Diagnostic Techniques

At our institution, initial imaging modalities in the evaluation of suspected or confirmed leaks are usually noninvasive, including high-resolution computed tomography (HRCT) and magnetic resonance cisternography (MRC). In complex or equivocal cases, more invasive techniques including computed tomography cisternography (CTC), contrast-enhanced magnetic resonance cisternography (CE-MRC), and radionuclide cisternography (RNC) are employed as problem-solving techniques (Table 5.1). Ultimately, the choice of imaging modality and diagnostic accuracy remains dependent on local experience, imaging expertise, and the technical capabilities at any individual institution.

Table 5.1 Proposed imaging algorithm for patients with confirmed CSF leak

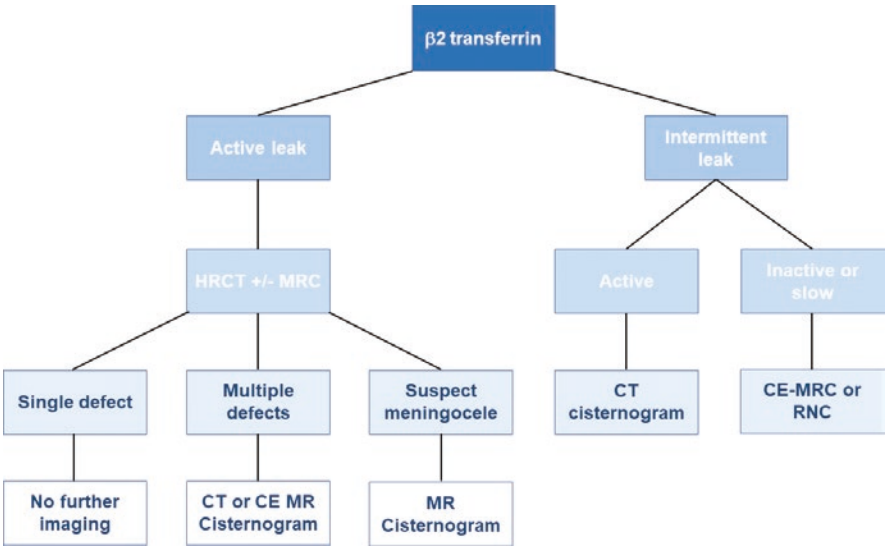

Computed Tomography

High-resolution CT (HRCT) of the paranasal sinuses and skull base is often the first-line imaging modality of choice in the setting of suspected CSF leak due to its relative clinical accessibility and short acquisition time. HRCT performed using submillimeter acquisition affords exquisite spatial resolution and superior delineation of osseous detail, making it ideal to identify potential regions of dehiscence of the anterior and posterolateral skull base [12–14]. In a recently meta-analysis, 12 published studies reported HRCT sensitivity over 80% in the identification of the site of a β2-transferrin-confirmed CSF leak [7]. Moreover, a recent investigation indicated that the size of the defect can be accurately predicted on HRCT to within 2 mm in 75% of cases [12] assuming minimum collimation and the ability to general multiplanar reformats. Adding to the potential utility of this technique, the identification of osseous dehiscence by HRCT is not dependent on the presence of an active leak at the time of imaging, making it ideal for the investigation of subtle abnormalities or slow-flowing leaks [11, 15]. Furthermore, dedicated HRCT of the paranasal sinuses and skull base affords the surgeon a detailed view of the remainder of the sinonasal cavity for surgical planning and intraoperative navigation during endoscopic repair [12, 14, 16].

HRCT performed for the identification of CSF leak should include minimum detector collimation, thin-section (0.5 mm or 0.625 mm) acquisition utilizing bone algorithms [1, 11, 17]. In general, axial images are considered superior for the evaluation of the vertically oriented structures of the skull base, including the posterior frontal and lateral sphenoid sinuses and in the evaluation of the mastoid air cells (Fig. 5.1). In distinction, coronal images offer advantage in the assessment of the

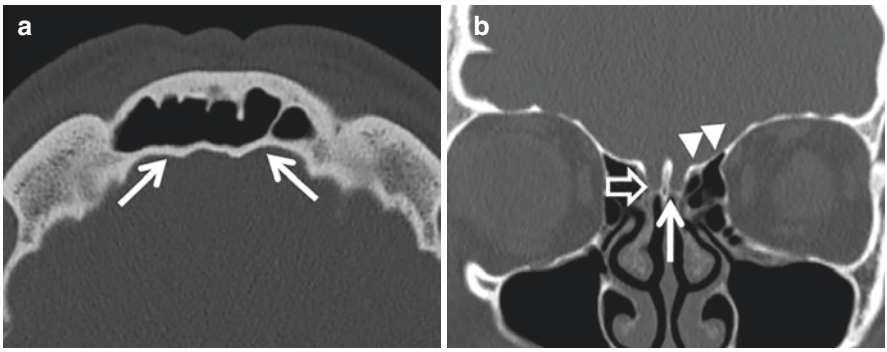

Fig. 5.1 High-resolution computed tomography (HRCT). Axial 0.625 mm direct acquisition (**a**) and reformatted coronal 1 mm (**b**) images of the anterior skull base obtained per HRCT protocol using bone algorithm reconstructions. In (**a**), axial views afford detailed evaluation of the vertically oriented components of the skull base, such as the posterior walls of the frontal sinus (arrows). Coronal reformats are ideally suited to assess the floor of the anterior cranial fossa, including common sites of CSF leak such as the olfactory fossa/cribriform plate (arrow), the lateral lamella (open arrow, shown near the attachment of the middle turbinate), and the fovea ethmoidalis (arrowheads)

longitudinally oriented cribriform plates, planum ethmoidale, planum sphenoidale, and temporal tegmen (Fig. 5.1). As such, historical acquisition parameters have included both axial and direct coronal planes for improved in-plane resolution, requiring prone positioning of the patient, significant neck extension within the gantry, and increased radiation dosage. Modern multi-detector CT now involves rapid, continuous volumetric acquisition with isotropic voxels, allowing for the creation of high-quality, high-resolution coronal and sagittal reformats from a single axial acquisition [1, 11]. Unless the location of a CSF leak is known, a thorough work up of CSF rhinorrhea requires HRCT imaging of the anterior, central, and posterolateral skull base as CSF leaking into the middle ear cavity can present as rhinorrhea via egress through the Eustachian tubes [18]. Therefore, the authors recommend a field-of-view inclusive of the sinonasal cavity, anterior and central skull base, and temporal bones for complete evaluation of suspected or confirmed CSF rhinorrhea.

Relative disadvantages of HRCT include the inability to assess for a concomitant dural defect in the setting of multiple regions of osseous thinning at the skull base. HRCT is also limited in the ability to discriminate between adjacent mucosal thickening and secretions from a suspected CSF collection in the paranasal sinuses [11, 16]. These limitations may contribute to the wide ranges of specificity of HRCT in the detection of a CSF leak reported in the literature, ranging from 57 to 100% [7, 19]. However, if only single osseous defect is identified on HRCT corresponding to the clinical symptoms, the patient can proceed to surgical repair without further imaging [12, 14].

Magnetic Resonance Cisternography

Magnetic resonance cisternography (MRC) is often performed as an adjunct or even a stand-alone imaging study in the setting of confirmed CSF leak due to superior soft tissue resolution and ability to increase the conspicuity of CSF based on the imaging technique utilized. Most MRC protocols exploit heavily T2-weighted (T2W) 3D-fast (turbo) spin echo (e.g., T2 SPACE, T2 CUBE) or steady-state-free precession (SSFP) sequences to highlight the intrinsic T2 prolongation of CSF relative to the adjacent neural and osseous elements, as well as facilitating the creation of multiplanar reformats from submillimeter acquisition [11, 20] (Fig. 5.2). In this manner, MRC can not only confirm but also identify the site of a CSF leak by visualizing a contiguous CSF column extending through a defect in the floor of the anterior cranial fossa, tegmen tympani, or tegmen mastoideum. Collectively, studies report a sensitivity of 56–94% for CSF leak detection, with a specificity of 57–100% [7].

A further advantage of MRC relative to HRCT is the ability to identify herniation of the meninges or neural elements (e.g., meningocele or meningoencephalocele) in association with an ongoing CSF leak [1, 11, 14]. Underlying meningoencephalocele should be considered in the setting of a skull base defect with downstream opacification of an adjacent sinus or mastoid air cell, particularly if the opacification

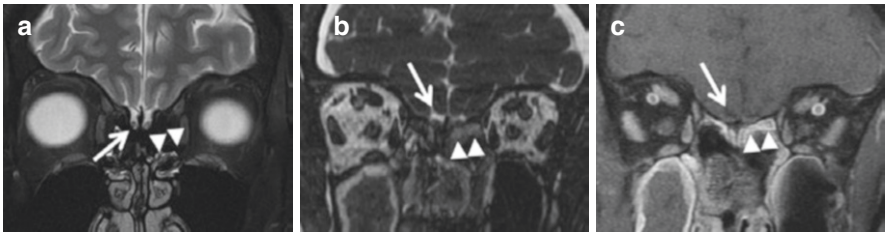

Fig. 5.2 Magnetic resonance cisternogram (MRC). Although various protocols exist, the mainstay of MRC is the use of a combination of multiplanar small field of view, thin section fast-spin-echo, and steady-state-free-precession (SSFP) imaging. In (**a**) coronal T2 fat-saturated images clearly depict the olfactory nerves in the olfactory groove (arrows), with easy differentiation from adjacent mucosal thickening of the ethmoid air cells (arrowheads). MRC performed to evaluate for recurrent leak after endoscopic nasal surgery (**b** and **c**) utilized both SSFP/FIESTA imaging (**b**) and thin section T1 fat-saturated post-contrast sequences (**c**) to clearly delineate the difference between native CSF signal (**b** and **c**, arrows) and adjacent mucosal thickening of the planum ethmoidale (**b** and **c**, arrowheads). No CSF leak was identified on the examination, and the patient continues to do well 2 years after surgery

is lobulated or anti-dependent. Although differentiation between fluid opacification and neural elements is often difficult by CT, the superior soft tissue resolution of MR easily distinguishes brain parenchyma from CSF, helping to aid surgical planning prior to repair (Fig. 5.2). The use of additional fast-spin echo and fast spoiled gradient-echo sequences, particularly with intravenous contrast and fat suppression, can further help identify potential complications related to CSF, such as retrograde meningitis and encephalitis.

One limitation of MRC is its dependence upon the presence of an active leak at the time of imaging to successfully identify the region of communication between the intracranial and extracranial compartments. Coupled with an inherently lower spatial resolution of the osseous skull base, many authors advocate use of both HRCT and MRC, with a combined reported accuracy of 92–100% in the current literature [21–23].

Contrast-Enhanced Cisternography

In contrast to the previously described imaging methodologies, contrast-enhanced CT and MR cisternography are invasive techniques, requiring the administration of intrathecal contrast, usually via lumbar puncture in the fluoroscopy suite. With improvements in both HRCT and MRC, intrathecal contrast-based imaging is utilized as a problem-solving tool at our institution, reserved for complex or equivocal cases after other imaging modalities have been employed.

CT cisternography (CTC) was previously the gold standard in the evaluation of potential CSF leaks, but now is predominantly used as a problem-solving technique, particularly to help pinpoint the site of an active leak in the setting of multiple

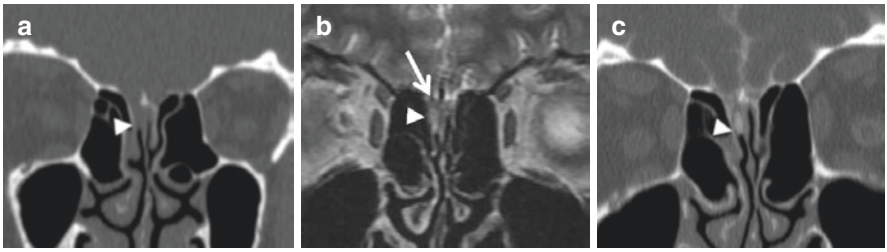

Fig. 5.3 Computed tomography cisternogram (CTC). 62-year-old patient presented with chronic but intermittent watery rhinorrhea, with β2 transferrin confirmed CSF leak at an outside institution. HRCT identified asymmetric opacification of the right superior meatus (**a**, arrowhead), although it was unclear if this was due to a low-lying right olfactory fossa or underlying osseous dehiscence. MRC revealed asymmetric opacification of the right superior meatus with otherwise appropriate localization of the right olfactory nerve (**b**, arrowhead). Of note, no clear CSF column could be identified on this study. In this setting, CTC was pursued as a problem-solving technique, demonstrating contrast accumulation through the right cribriform plate into the right nasal cavity (**c**, arrowhead) confirming CSF leak in this location

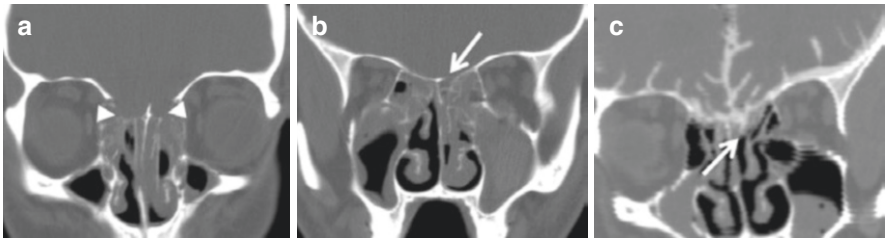

Fig. 5.4 CTC in the setting of complex skull base findings. In this patient with a history of prior facial trauma and β2 transferring positive rhinorrhea, multiple regions of thinning of the anterior skull base structures were noted, including involving the bilateral lateral lamella (**a**, arrowheads) and the left fovea ethmoidalis (**b**, arrow). Subsequent CTC performed with provocative maneuvering revealed contrast extravasation through the left fovea defect (**c**, arrow) as the site of the patient's ongoing CSF leak

osseous defects [14, 24] (Figs. 5.3 and 5.4). CTC protocol involves obtaining HRCT in both the prone and supine positions through the region of interest before and after low osmolality intrathecal contrast material is introduced. One advantage to CTC is the ability to perform provocative maneuvers at the time of imaging, such as sneezing or head hanging, to attempt to improve delineation of a leak. Evaluation of the obtained imaging requires comparison of the pre- and post-contrast scans, with a positive result considered if there is an increase in the attenuation of an opacified structure (sinus, nasal cavity, middle ear, etc.) adjacent to a skull base defect 50% or more above the baseline on the noncontrast examination [14]. The utility of a CTC is limited to patients in whom an active leak is present or elicited by provocative maneuvers. Additional pitfalls of this technique can include obscuration of small

leaks by adjacent sclerotic changes of the paranasal sinuses or high-density, inspissated secretions, as well as the presence of blood. In combination, these factors may account for some degree of the disparity of reported sensitivities, ranging from 33% to 100% [7, 19, 22].

Intrathecal, contrast-enhanced techniques can also be combined with the MRC technique, utilizing thin-section, T1-weighted sequences obtained in multiple planes after the administration of gadolinium-based contrast. Similar to CTC, a positive study demonstrates contrast extravasation through an osseous and dural defect of the skull base and must be interpreted in conjunction with HRCT. Studies have shown enhanced sensitivity for detection of CSF leaks compared to both HRCT and standard MRC, with up to 100% sensitivity for high-flow leaks and 60% to 70% sensitivity for slow-flow leaks [20, 25, 26]. Some of this improved sensitivity may stem from the ability to perform delayed imaging up to 24 h after gadolinium administration, which can be particularly useful in slow-flowing or intermittent leaks [26]. As with all MR-based protocols, superior soft tissue resolution and increased conspicuity of CSF afford the ability to detect concomitant meningoceles as well as improved discrimination of leaking contrast from adjacent sclerotic or hypertrophied bony structures compared to CTC. Although several studies indicate good safety data using low-dose intrathecal gadolinium in other countries, intrathecal administration remains an off-label use of gadolinium by the US Food and Drug Administration (FDA), and long-term safety studies are still pending. As such, given the invasive nature of the study, the known neurotoxicity of gadolinium in high doses, and current off-label use, selective employment of this technique as a problem-solving tool only is recommended and only after thorough off-label use consent.

Nuclear Medicine Cisternography

Radionuclide cisternography (RNC) is a nuclear medicine diagnostic examination involving the intrathecal administration of technetium-99 or indium-111 radiotracer. Multiple pledglets are introduced to the nasal cavity followed by placing the patient in the Trendelenburg position to facilitate craniad tracer flow [1, 16]. Pledglet radioactivity is measured after 24 to 48 h to confirm the presence of a CSF leak, with a positive study heralded by a pledglet to serum plasma tracer ratio of 2:1 or 3:1 [1]. RNC is limited to the detection of active leaks and only offers minimal, if any, information about leak location given the inherent mixing of nasal secretions from side to side and the possibility of CSF rhinorrhea stemming from an underlying temporal bone process [1, 11, 14]. For these reasons, and due to its invasive nature, RNC is only selectively employed at our institution as a problem-solving measure for CSF leak confirmation.

Imaging Findings of CSF Leak

Imaging hallmarks of CSF leak on HRCT include an osseous defect in the skull base associated with an air-fluid level or opacification of the contiguous sinus, mastoid air cells, or middle ear cavity. The most common location for a skull base CSF leak is at the cribriform plate although several additional locations are also commonly implicated, including the anterior ethmoid, posterior ethmoid, sphenoid, and frontal sinuses [1] (Fig. 5.5). CSF leaks from the temporal bone tegmen are relatively less common but should be included in imaging protocol as CSF leakage into

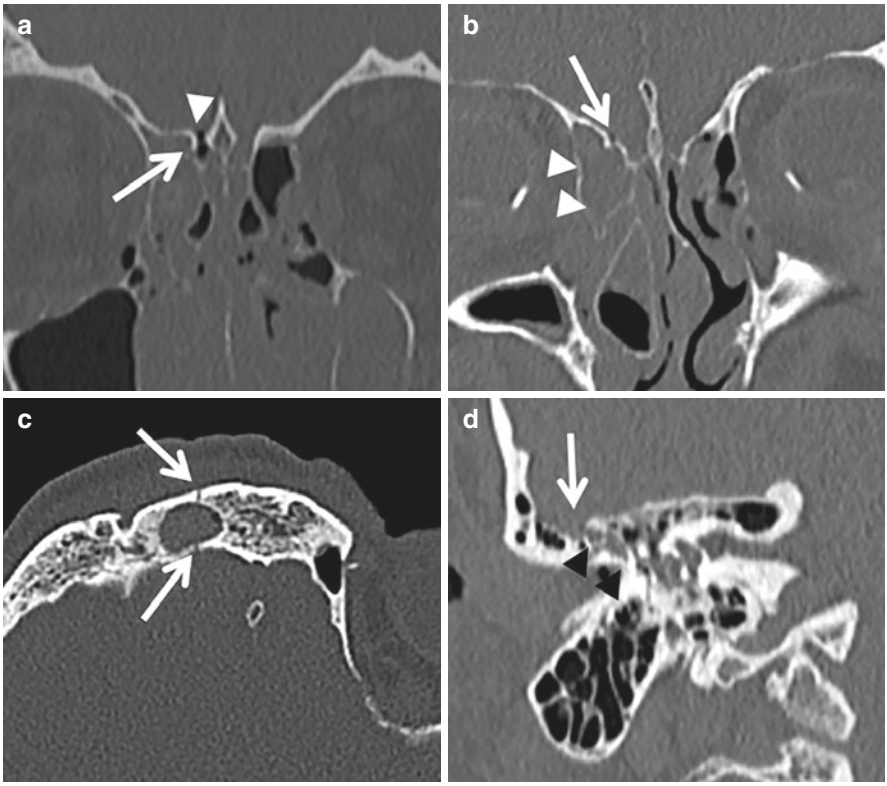

Fig. 5.5 Common sites of traumatic CSF leaks on HRCT. In (**a**), 1 mm bone algorithm coronal reformats clearly elucidate a focal region of pneumocephalus (arrowhead) adjacent to an otherwise subtle fracture of the right lateral lamella near the insertion of the middle turbinate. Focal pneumocephalus also heralds a subtle, minimally displaced fracture of the right fovea ethmoidalis (**b**, arrow) with associated CSF leak suspected based on downstream opacification of the adjacent superior ethmoid air cell (**b**, arrowheads). Bone algorithm axial 0.625 mm acquisition easily identifies a nondisplaced fracture extending through the anterior and posterior walls of the right frontal sinus (**c**, arrows) in the setting of facial trauma. In (**d**) coronal 1 mm bone algorithm reformats successfully resolve a mildly displaced fracture of the right tegmen mastoideum (arrow) with downstream opacification of the right-sided mastoid air cells, raising concern for post-traumatic CSF leak (arrowheads)

the middle ear can also manifest as rhinorrhea via egress through the Eustachian tubes [11, 14, 18] (Fig. 5.5). Anterior skull base defects are usually adjacent to the vertical insertion of the middle turbinate or at the lateral lamella, although normal thinning of these structures can make specific leak site detection difficult [1]. Identification is aided by comparing to the contralateral side, scrutinizing for subtle associated pneumocephalus adjacent to a fracture line, as well as identifying asymmetric mucosal thickening or soft tissue opacification beneath a suspected osseous defect as the first sign of an underlying meningoencephalocele (Figs. 5.6 and 5.7).

As adjunct imaging, or in the case of suspected meningoencephalocele, MRC may further help localize the leak by identifying a contiguous CSF column extending through a deficiency in the skull base and adjacent dura (Fig. 5.6), although this is contingent upon an active leak being present at the time of imaging. Further multiplanar T1- and T2-weighted imaging of the skull base is essential to detect the presence of an underlying meningocele/meningoencephalocele. Other indirect signs of CSF leak can also be revealed by MR, including variable degrees of encephalomalacia associated with an ongoing leak [11] (Fig. 5.6), associated dural enhancement (in the case of concurrent intravenous contrast administration), as well as the identification of potential intracranial complications, including meningitis/cerebritis (Fig. 5.8). Contrast-enhanced CT and MR cisternography evaluations are both based on identification of extravasated contrast via an osteodural defect in the skull base, often quantified in comparison to pre-contrast images, as previously described.

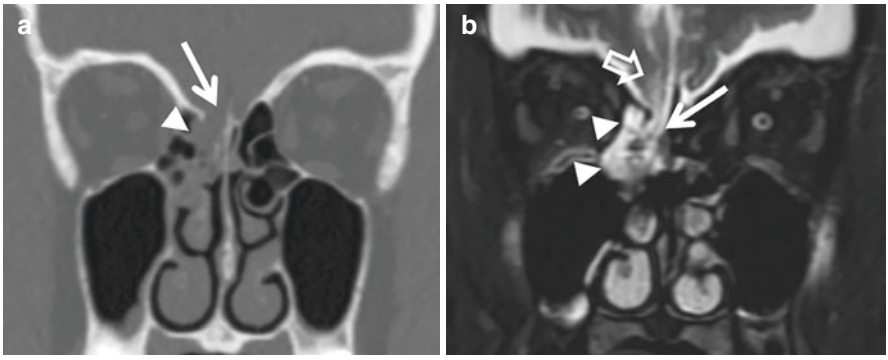

Fig. 5.6 Traumatic meningoencephalocele. 35-year-old male presents with new-onset seizures and watery nasal discharge for 1 year after assault. HRCT reveals focal dehiscence of the right cribriform plate (**a**, arrow) with polypoid opacification of the downstream ethmoid air cell (**a**, arrowhead). Concern for CSF leak and associated meningocele was raised and confirmed on MRC, with T2 fat-saturated sequences revealing herniation of the right gyrus rectus through the osteodural defect (**b**, arrow) and contiguous CSF column extending into the superior ethmoid air cells (**b**, arrowheads). Note associated gliosis of the right gyrus rectus, potentially contributing to the patient's ongoing seizure activity (**b**, open arrows)

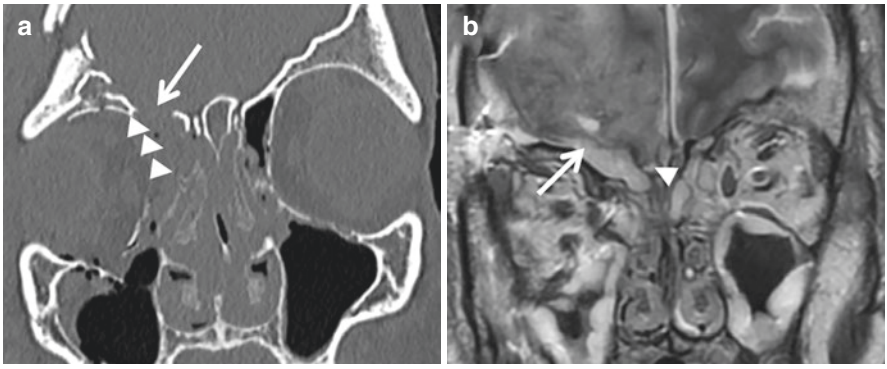

Fig. 5.7 Traumatic meningoencephalocele. In (**a**) 1 mm bone algorithm coronal reformats reveal comminuted fracture deformity of the superior, medial, and inferior right orbit extending through the floor of the frontal sinus and fovea ethmoidalis (**a**, arrow). Asymmetric opacification of the right superior meatus and anterior ethmoid air cells (**a**, arrowheads) raised concern for ongoing CSF leak and meningoencephalocele given proximity to the right frontal lobe. Subsequent MRC confirmed herniation of the adjacent anteroinferior frontal convexities into the frontal sinus defect (coronal T2 imaging in **b**, arrow) and into the olfactory fossa (**b**, arrowheads). Subsequent endoscopic and open repair of the skull base was performed with frankly gliotic brain noted herniating through the osteodural defect, which was successfully resected

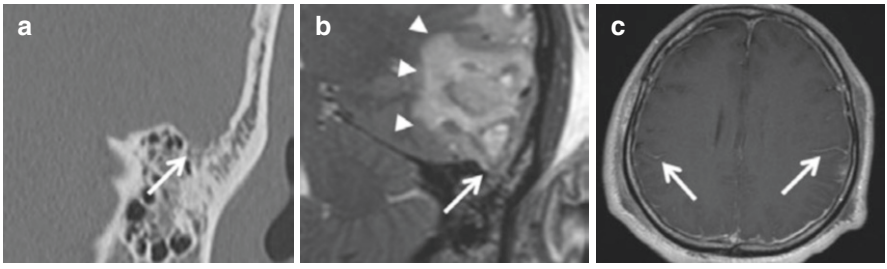

Fig. 5.8 Traumatic CSF leak with associated meningitis. 55-year-old male presenting as transfer from outside institution 1 month after left-sided head strike with persistent left-sided ear pain and constitutional symptoms. HRCT at our institution revealed a previously overlooked, subtle region of dehiscence of the left tegmen mastoideum (coronal reformats in **a**, arrow), prompting evaluation by MRC. In (**b**) T2 CUBE sequences were employed demonstrating a subtle meningoencephalocele through the queried defect (**b**, arrows). MRC also revealed asymmetric edema within the left inferolateral temporal lobe (**b**, arrowheads) with associated enhancement of the leptomeninges (axial T1 post-contrast in **c**, arrows) raising concern for superimposed meningitis due to ascending infection from the left middle ear cavity, later confirmed by lumbar puncture

With these general principles in mind, it is important to note that the imaging appearance of a CSF leak is dependent upon the underlying etiology, whether traumatic, iatrogenic, spontaneous, or secondary to underlying neoplastic, congenital, or infectious causes.

Traumatic CSF Leaks

The majority of skull base CSF leaks are associated with traumatic injuries, with 10% to 30% of skull base fractures complicated by concomitant CSF leak [14, 16, 27]. Tightly adherent dura along the inherently thin cribriform plates and planum ethmoidale/sphenoidale may explain the propensity for comminuted anterior cranial fossa fractures to result in CSF leak, although CSF from fractures of the posterior frontal sinus, lateral walls of the sphenoid sinus, or even the sella turcica have also been reported (Fig. 5.5). CSF leak frequency ranges from 11 to 45% of patients with underlying temporal bone fractures, more often in the setting of otic capsule violation [28]. Although displaced or comminuted fractures are rarely a clinical or diagnostic dilemma, subtle or nondisplaced fractures can be overlooked by routine CT; in this setting, the presence of intracranial pneumocephalus can be the first clue for a subtle osseous traumatic injury and should prompt careful interrogation of the adjacent skull base and/or repeat evaluation with HRCT (Fig. 5.5).

Iatrogenic CSF Leaks

CSF leak is a known complication of both neurosurgical and otolaryngologic procedures, with a reported overall incidence of 14% via endoscopic and endonasal approaches to the anterior and central skull base [29] (Fig. 5.9). As such, the timely reporting of variant anatomy of the anterior cranial fossa and central skull base is of critical importance on presurgical HRCT, including the Keros classification of the olfactory fossa and any associated asymmetry of the cribriform plate [30]. Variant sphenoid sinus pneumatization should also be reported, as well as any extension anteriorly into the clinoid process, laterally into the sphenoid wing, inferiorly into

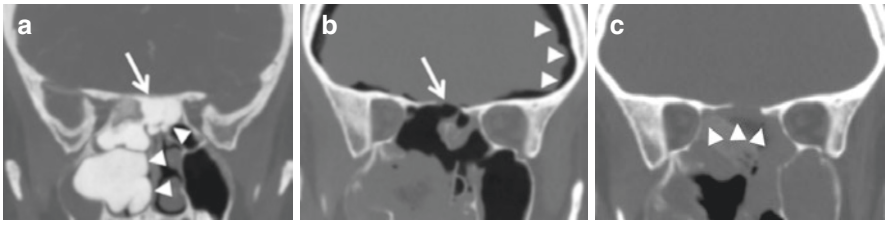

Fig. 5.9 Iatrogenic CSF leak. In (**a**) coronal reformatted images from CT angiography performed for surgical planning prior to resection of a transpatial sinonasal osteoma (**a**, arrowheads) demonstrating close approximation with and thinning of the planum sphenoidale (**a**, arrow). Although initially asymptomatic, the patient began to complain of watery rhinorrhea and worsening headaches on postoperative day 2. Subsequent HRCT demonstrated a focal osseous dehiscence of the left planum sphenoidale (**b**, arrow) with progressive pneumocephalus (**b**, arrowheads). Given concern for ongoing CSF leak, surgical exploration was performed revealing multiple dural tears and exposed brain in the region of osseous dehiscence, which was then repaired with an extensive nasoseptal flap (**c**, arrowheads)

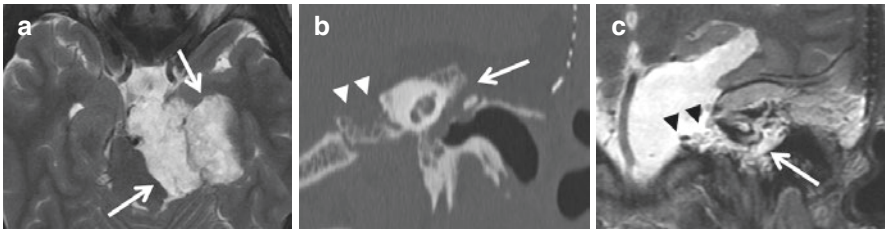

Fig. 5.10 Postsurgical CSF leak. 30-year-old female presented with copious clear rhinorrhea after left translabyrinthine approach epidermoid resection (show in **a**, axial T2 sequence, arrows). HRCT revealed several areas of potential osseous dehiscence involving the tegmen tympani (**b**, arrow), although fat-grafting material appeared to approximate the potential defect in this location. Instead, there was an additional 10 mm region of dehiscence of the left petrous ridge (**b** and **c**, arrowheads) with apparent contiguous CSF column extending from this defect through to the left middle ear cavity (T2-weighted coronal image in **c**, arrow), subsequently confirmed as the site of ongoing leak by surgical re-exploration

the pterygoid plate, or posteriorly into the clivus, as associated bony thinning can increase the risk of postoperative CSF leak [31]. Most iatrogenic leaks occur within the first 2 postoperative weeks and resolve spontaneously [14]; if repair is indicated, typically only preoperative HRCT is required as the location of the leak is assumed at the surgical site, although initial evaluation can be difficult in the immediate post-operative setting given adjacent post-surgical material and hemorrhage (Fig. 5.10).

Secondary CSF Leaks

In the absence of trauma or prior surgery, there are many additional potential causative etiologies of CSF leak at the skull base, including sinonasal or primary skull base malignancy (Fig. 5.11), prior radiation therapy/osteoradionecrosis, or congenital abnormalities, including encephaloceles, persistent craniopharyngeal canal, or primary empty sella syndrome.

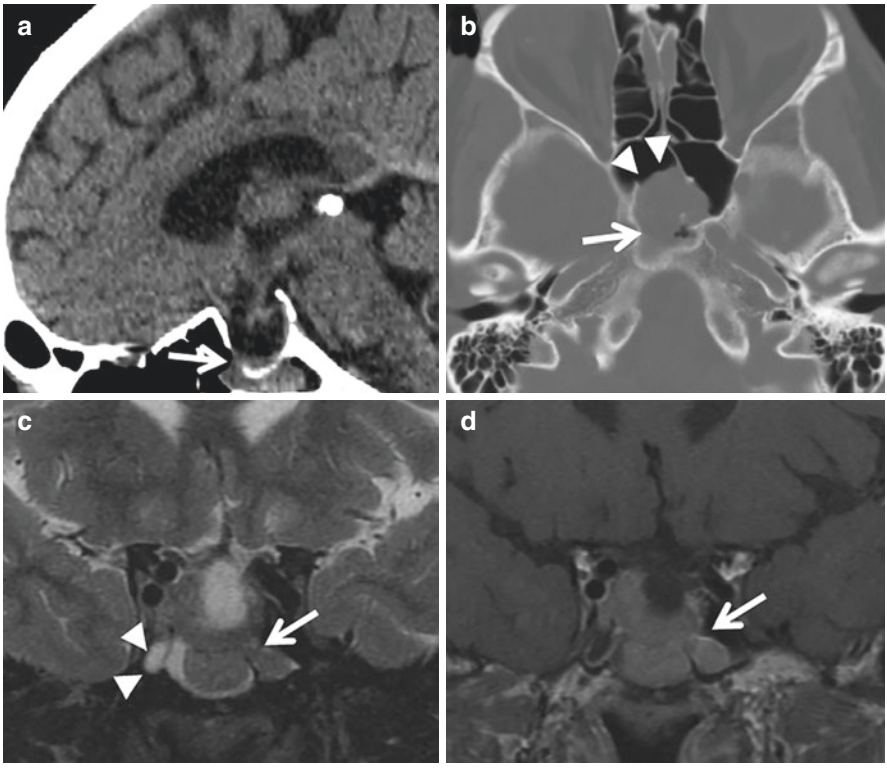

Fig. 5.11 CSF rhinorrhea related to neoplasia. 53-year-old female presenting with positional headaches and bilateral rhinorrhea. Screening head CT revealed a widened sella with a focal osseous defect of the anterior sella turcica and posterior wall of the sphenoid sinus (**a** and **b**, arrowheads). Internally, a polypoid, anti-dependent mass was noted without definite continuity with the brain parenchyma of the medial temporal lobes (**b**, arrowheads). Follow-up MRI demonstrated transpatial, T2 hypointense mass extending through the anteroinferior aspect of the sella turcica with low-level internal enhancement (coronal T2 fat-saturated in C and T1 post-contrast in **d**, arrows), compatible with underlying pituitary macroadenoma. Although no definite contiguous CSF column was identified through the osteodural defect of the central skull base, T2 hyperintense fluid in the adjacent sphenoid sinus (**c**, arrowheads) raised suspicion for subtle associated CSF leak as the cause of the patient's ongoing rhinorrhea

Spontaneous CSF Leaks

The last several decades have seen increased prevalence of idiopathic intracranial hypertension (IIH), a headache syndrome characterized by supranormal intracranial pressure without clear cause, classically seen in overweight women associated with visual disturbance, papilledema, and other potential neurologic stigmata [32]. Spontaneous CSF leaks are becoming a frequent presentation of IIH and one of the most common indications for imaging in the setting of CSF leak [33, 34]. In this cohort of patients, it is proposed that elevated intracranial pressures leads to increased magnitude of dural pulsations, weakening the

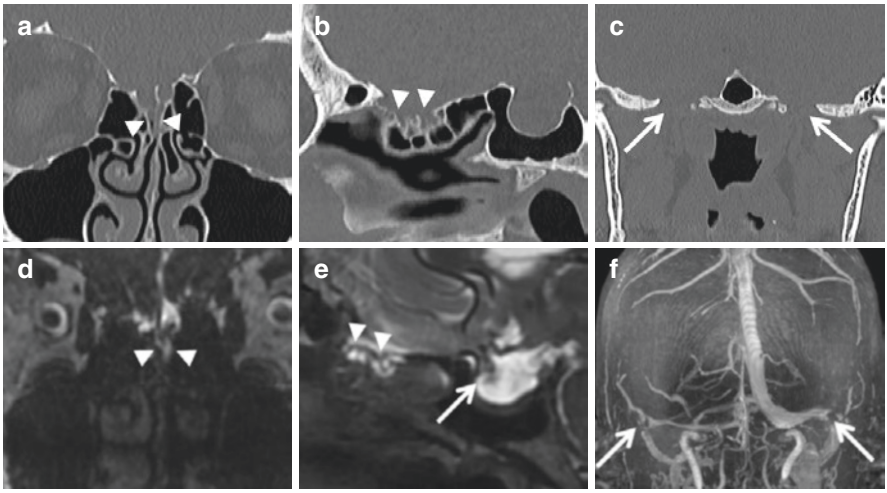

Fig. 5.12 Spontaneous CSF leak in the setting of idiopathic intracranial hypertension. 59-year-old female presenting with postural headaches and intermittent left-sided rhinorrhea. HRCT demonstrated thinning of both cribriform plates (**a**, arrowheads) with subtle downstream opacification of the left greater than right superior nasal cavity. Associated widening of the sella turcica (**b**, arrow) and foramen ovale (**c**, arrows) raised suspicion for elevated intracranial pressures. MRC (sagittal T2 CUBE sequences in **c** and **d**) confirmed active CSF leak on the left with contiguous CSF signal extending through the osteodural defect of the left cribriform plate (**c**, arrowheads). Associated meningoencephalocele with herniation of the olfactory bulb through the defect in the cribriform plate is best depicted on sagittal reformats (**d**, arrowheads). Additional stigmata of IIH were identified on the MRC, including widening of the sella turcica with flattening of the pituitary gland (**e**, arrow) and stenosis of the dural venous sinuses at the level of the transverse-sigmoid junctions (**f**, post-contrast MR venogram in **e**, arrows)

osseous skull base and resulting in multiple regions of thinning and dehiscence seen on HRCT [35, 36]. Loss of osseous integrity, coupled with elevated intracranial pressures, allows for the formation of multiple arachnoid pits/granulations and, eventually, dural tears with associated CSF leak. Although imaging findings are not in the diagnostic criteria for IIH, there are several MR imaging features that have been associated with IIH in the literature, including an expanded sella with a partially empty configuration, optic nerve sheath enlargement/tortuosity, flattening of the posterior globe, and/or papilledema [13, 37] (Figs. 5.12 and 5.13). Other works have described stenosis between the junction of the transverse and sigmoid sinuses as the most specific feature of IIH, although it remains unclear if this is a causative agent or secondary finding in this clinical diagnosis [38] (Fig. 5.12). Nevertheless, these imaging features in conjunction with clinical signs of papilledema and elevated opening pressure on lumbar puncture are strongly suggestive of the diagnosis of IIH. Given the propensity for multifocal regions of osseous thinning and the increased risk of meningocele/meningoencephalocele formation, patients with suspected or confirmed IIH often require multimodal imaging work up including both HRCT and MRC prior to any elective intervention.

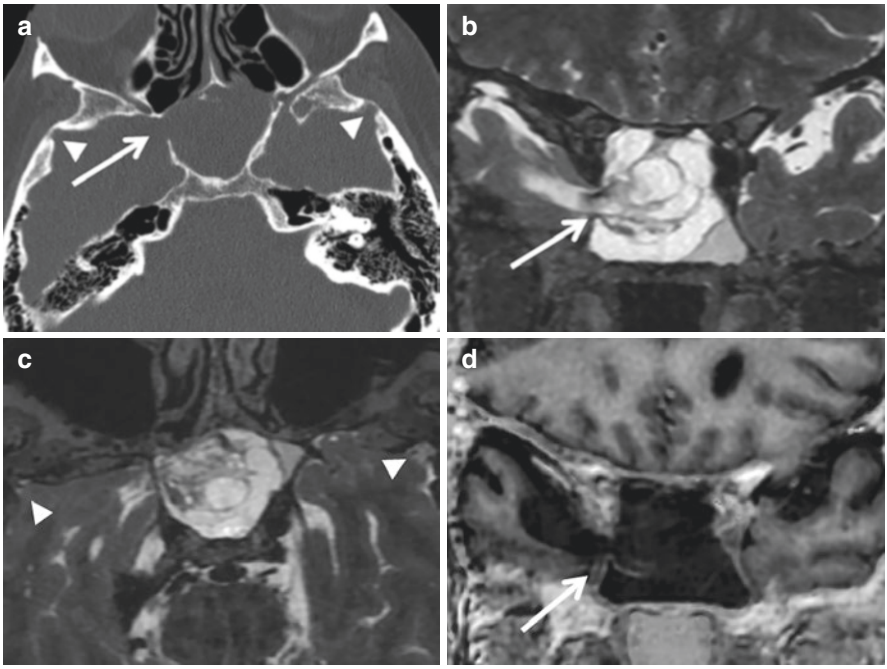

Fig. 5.13 Spontaneous CSF leak in the setting of idiopathic intracranial hypertension. 70-year-old female with 3-month history of intermittent vertigo, sinonasal congestion, and watery nasal discharge. An 8 mm defect was noted in the lateral wall of the right sphenoid sinus on HRCT (**a**, arrow) with polypoid opacification of the sinus lumen (**a**, open arrow) concerning for CSF leak and possible meningoencephalocele. Subsequent MRC demonstrated a large meningoencephalocele extending through the sphenoid sinus defect (**b** and **d**, arrows) with contiguous opacification of the sphenoid sinus with CSF as demonstrated by uniformly T2 hyperintense signal on heavily T2-weighted volumetric sequences (**b**). For this example, phase-sensitive-inversion-recovery (PSIR) sequences were also performed (**d**) which display native subarachnoid CSF signal as hypointense relative to the adjacent bony structures, which can be helpful in the discrimination between CSF and marrow signal. Also note additional focal regions of bony thinning of the inner margin of the middle cranial fossa (on HRCT in **a**, arrowheads), revealed as additional small meningoencephaloceles (**b**, arrowheads), in keeping with the diagnosis of IIH

Pitfalls and Mimics

There are numerous challenges in the imaging evaluation of patients with suspected or confirmed CSF rhinorrhea and otorrhea. Some of the more frequently encountered include:

– MRC, CTC, and contrast-enhanced MRC are dependent upon the presence of an active CSF leak at the time of imaging and, as such, may fail to detect intermittent or very-slow flow leaks at the time of imaging.
– Although HRCT can identify bony defects regardless of leak activity, thinning and irregularity of the skull base structures of the anterior and middle cranial

fossa are a relatively common finding in the population in the absence of clinical concern for CSF leak.

– Particularly in the setting of IIH or polytrauma, multiple osseous defects, and even multiple meningoceles, may be present in one patient, making the identification of the true site of active leakage difficult on HRCT. MR cisternogram can be helpful in this setting, but can result in the occasional false negative if the patient is not leaking at the time of imaging. In these cases, consideration of CTC or contrast-enhanced MRC is recommended, potentially with provocative maneuvers or delayed imaging, as problem-solving tools for better localization.
– Evaluation of contrast extravasation using CTC in the postoperative setting can be obscured by other high-density components, including hypertrophied osseous structures, inspissated secretions/blood products, and granulation tissue. Comparison between pre- and post-contrast images and careful windowing using soft tissue algorithms can be helpful to discriminate between artifact and true egress of contrast.

Although there is no real differential diagnosis for an underlying CSF leak, there are several imaging findings on HRCT that may mimic the opacification pattern of a CSF leak, yet belie a more insidious process. Ostiomeatal unit pattern sinonasal inflammatory disease, particularly if long standing, can result in various degrees of neo-osteogenesis and osseous thinning, although intact periosteum may be in place in the absence of symptoms referable to CSF rhinorrhea. Both CSF leaks and malignancy can present as unilateral opacification of the sinonasal cavity; in this case, frank osseous destruction of the intervening bony boundaries can tip the radiologist toward a diagnosis of underlying malignancy, which is easily confirmed by MRI (Fig. 5.14).

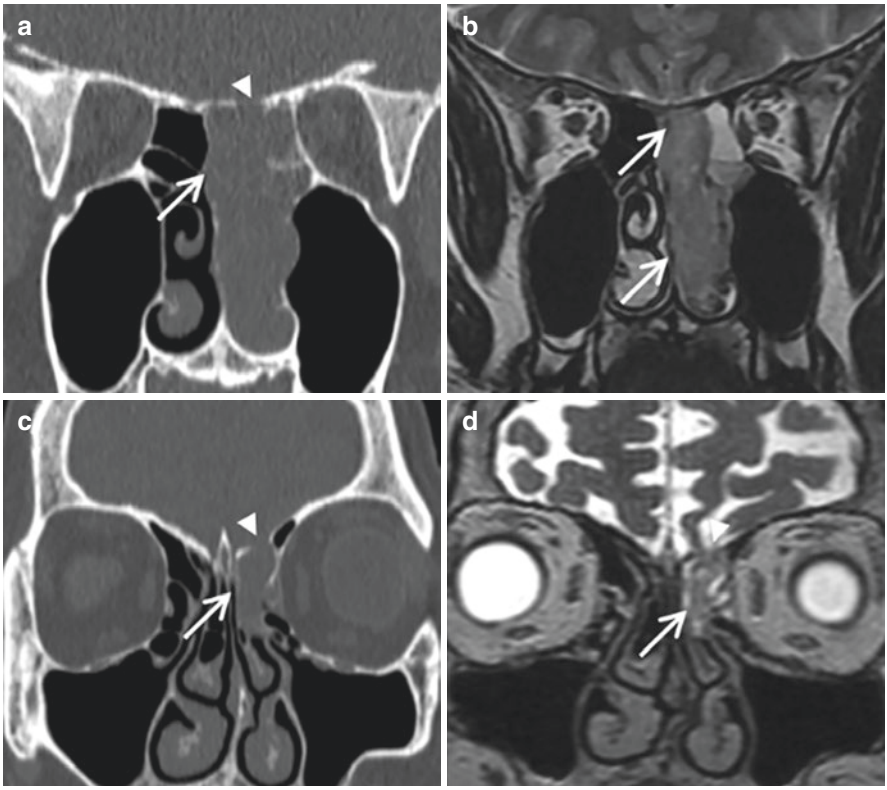

Fig. 5.14 Mimics of CSF leak. Coronal bone algorithm reformatted HRCT images (**a** and **c**) on two different patients, both of which demonstrate dehiscence of the floor of the anterior cranial fossa (**a** and **c**, arrowheads) with associated downstream opacification of the adjacent left ethmoid air cells (**a** and **c**, arrows). However, the follow-up MRI (coronal T2 weighted in **b**) in this patient with several months of long-standing left-sided nasal obstruction revealed a T2 hypointense mass extending from the superior meatus through the nasal cavity (**b**, arrows), now biopsy confirmed sinonasal neuroectodermal tumor (SNEC). In distinction, the patient in **c** presented with a history of remote trauma, chronic rhinorrhea, and recurrent meningitis, raising suspicion for an underlying CSF leak consequent to a previously undiagnosed fracture of the left lateral lamella. T2-CUBE sequences (coronal in **d**) were confirmatory, detailing a post-traumatic meningoencephalocele extending into the left anterior ethmoid air cells (**d**, arrow)

References

1. Lloyd KM, DelGaudio JM, Hudgins PA. Imaging of skull base cerebrospinal fluid leaks in adults. Radiology. 2008;248(3):725–36.
2. Daudia A, Biswas D, Jones NS. Risk of meningitis with cerebrospinal fluid rhinorrhea. Ann Otol Rhinol Laryngol. 2007;116(12):902–5.
3. Aarabi B, Leibrock LG. Neurosurgical approaches to cerebrospinal fluid rhinorrhea. Ear Nose Throat J. 1992;71(7):300–5.

4. Eftekhar B, Ghodsi M, Nejat F, Ketabchi E, Esmaeeli B. Prophylactic administration of ceftriaxone for the prevention of meningitis after traumatic pneumocephalus: results of a clinical trial. J Neurosurg. 2004;101(5):757–61.
5. Eljamel MS, Foy PM. Acute traumatic CSF fistulae: the risk of intracranial infection. Br J Neurosurg. 1990;4(5):381–5.
6. Friedman JA, Ebersold MJ, Quast LM. Post-traumatic cerebrospinal fluid leakage. World J Surg. 2001;25(8):1062–6.
7. Oakley GM, Alt JA, Schlosser RJ, Harvey RJ, Orlandi RR. Diagnosis of cerebrospinal fluid rhinorrhea: an evidence-based review with recommendations. Int Forum Allergy Rhinol. 2016;6(1):8–16.
8. Wang EW, Vandergrift WA, Schlosser RJ. Spontaneous CSF leaks. Otolaryngol Clin N Am. 2011;44(4):845–56. vii
9. Warnecke A, Averbeck T, Wurster U, Harmening M, Lenarz T, Stöver T. Diagnostic relevance of beta2-transferrin for the detection of cerebrospinal fluid fistulas. Arch Otolaryngol Head Neck Surg. 2004;130(10):1178–84.
10. Zapalac JS, Marple BF, Schwade ND. Skull base cerebrospinal fluid fistulas: a comprehensive diagnostic algorithm. Otolaryngol Head Neck Surg. 2002;126(6):669–76.
11. Hiremath SB, Gautam AA, Sasindran V, Therakathu J, Benjamin G. Cerebrospinal fluid rhinorrhea and otorrhea: a multimodality imaging approach. Diagn Interv Imaging. 2019;100(1):3–15.
12. La Fata V, McLean N, Wise SK, DelGaudio JM, Hudgins PA. CSF leaks: correlation of high-resolution CT and multiplanar reformations with intraoperative endoscopic findings. AJNR Am J Neuroradiol. 2008;29(3):536–41.
13. Alonso RC, de la Peña MJ, Caicoya AG, Rodriguez MR, Moreno EA, de Vega Fernandez VM. Spontaneous skull base meningoencephaloceles and cerebrospinal fluid fistulas. Radiographics. 2013;33(2):553–70.
14. Reddy M, Baugnon K. Imaging of cerebrospinal fluid rhinorrhea and otorrhea. Radiol Clin N Am. 2017;55(1):167–87.
15. Lloyd MN, Kimber PM, Burrows EH. Post-traumatic cerebrospinal fluid rhinorrhoea: modern high-definition computed tomography is all that is required for the effective demonstration of the site of leakage. Clin Radiol. 1994;49(2):100–3.
16. Prosser JD, Vender JR, Solares CA. Traumatic cerebrospinal fluid leaks. Otolaryngol Clin N Am. 2011;44(4):857–73. vii
17. Schuknecht B, Simmen D, Briner HR, Holzmann D. Nontraumatic skull base defects with spontaneous CSF rhinorrhea and arachnoid herniation: imaging findings and correlation with endoscopic sinus surgery in 27 patients. AJNR Am J Neuroradiol. 2008;29(3):542–9.
18. Saim L, McKenna MJ, Nadol JB. Tubal and tympanic openings of the peritubal cells: implications for cerebrospinal fluid otorhinorrhea. Am J Otol. 1996;17(2):335–9.
19. Stone JA, Castillo M, Neelon B, Mukherji SK. Evaluation of CSF leaks: high-resolution CT compared with contrast-enhanced CT and radionuclide cisternography. AJNR Am J Neuroradiol. 1999;20(4):706–12.
20. Algin O, Hakyemez B, Gokalp G, Ozcan T, Korfali E, Parlak M. The contribution of 3D-CISS and contrast-enhanced MR cisternography in detecting cerebrospinal fluid leak in patients with rhinorrhoea. Br J Radiol. 2010;83(987):225–32.
21. Shetty PG, Shroff MM, Sahani DV, Kirtane MV. Evaluation of high-resolution CT and MR cisternography in the diagnosis of cerebrospinal fluid fistula. AJNR Am J Neuroradiol. 1998;19(4):633–9.
22. Mostafa BE, Khafagi A. Combined HRCT and MRI in the detection of CSF rhinorrhea. Skull Base. 2004;14(3):157–62; discussion 62
23. Tuntiyatorn L, Laothammatas J. Evaluation of MR cisternography in diagnosis of cerebrospinal fluid fistula. J Med Assoc Thail. 2004;87(12):1471–6.
24. Vimala LR, Jasper A, Irodi A. Non-invasive and minimally invasive imaging evaluation of CSF Rhinorrhoea - a retrospective study with review of literature. Pol J Radiol. 2016;81:80–5.

25. Selcuk H, Albayram S, Ozer H, Ulus S, Sanus GZ, Kaynar MY, et al. Intrathecal gadolinium-enhanced MR cisternography in the evaluation of CSF leakage. AJNR Am J Neuroradiol. 2010;31(1):71–5.
26. DelGaudio JM, Baugnon KL, Wise SK, Patel ZM, Aiken AH, Hudgins PA. Magnetic resonance cisternogram with intrathecal gadolinium with delayed imaging for difficult to diagnose cerebrospinal fluid leaks of anterior skull base. Int Forum Allergy Rhinol. 2015;5(4):333–8.
27. Baugnon KL, Hudgins PA. Skull base fractures and their complications. Neuroimaging Clin N Am. 2014;24(3):439–65, vii-viii
28. Johnson F, Semaan MT, Megerian CA. Temporal bone fracture: evaluation and management in the modern era. Otolaryngol Clin N Am. 2008;41(3):597–618. x
29. Naunheim MR, Sedaghat AR, Lin DT, Bleier BS, Holbrook EH, Curry WT, et al. Immediate and delayed complications following endoscopic Skull Base surgery. J Neurol Surg B Skull Base. 2015;76(5):390–6.
30. García-Garrigós E, Arenas-Jiménez JJ, Monjas-Cánovas I, Abarca-Olivas J, Cortés-Vela JJ, De La Hoz-Rosa J, et al. Transsphenoidal approach in endoscopic endonasal surgery for Skull Base lesions: what radiologists and surgeons need to know. Radiographics. 2015;35(4):1170–85.
31. Hamid O, El Fiky L, Hassan O, Kotb A, El Fiky S. Anatomic variations of the sphenoid sinus and their impact on trans-sphenoid pituitary surgery. Skull Base. 2008;18(1):9–15.
32. Kilgore KP, Lee MS, Leavitt JA, Mokri B, Hodge DO, Frank RD, et al. Re-evaluating the incidence of idiopathic intracranial hypertension in an era of increasing obesity. Ophthalmology. 2017;124(5):697–700.
33. Pérez MA, Bialer OY, Bruce BB, Newman NJ, Biousse V. Primary spontaneous cerebrospinal fluid leaks and idiopathic intracranial hypertension. J Neuroophthalmol. 2013;33(4):330–7.
34. Tam EK, Gilbert AL. Spontaneous cerebrospinal fluid leak and idiopathic intracranial hypertension. Curr Opin Ophthalmol. 2019;30(6):467–71.
35. Stevens SM, Rizk HG, Golnik K, Andaluz N, Samy RN, Meyer TA, et al. Idiopathic intracranial hypertension: contemporary review and implications for the otolaryngologist. Laryngoscope. 2018;128(1):248–56.
36. O'Connell BP, Stevens SM, Xiao CC, Meyer TA, Schlosser RJ. Lateral Skull Base attenuation in patients with anterior cranial fossa spontaneous cerebrospinal fluid leaks. Otolaryngol Head Neck Surg. 2016;154(6):1138–44.
37. Bathla G, Moritani T. Imaging of cerebrospinal fluid leak. Semin Ultrasound CT MR. 2016;37(2):143–9.
38. Farb RI, Vanek I, Scott JN, Mikulis DJ, Willinsky RA, Tomlinson G, et al. Idiopathic intracranial hypertension: the prevalence and morphology of sinovenous stenosis. Neurology. 2003;60(9):1418–24.